Supporting Information

Spectral Properties and Energy Transfer Between $Ce^{3+} \rightarrow Yb^{3+}$ in the $Ca_3Sc_2Si_3O_{12}$ Host: Is It an Electron Transfer Mechanism?

Lei Zhou[†], Peter A. Tanner[*‡], Lixin Ning[§], Weijie Zhou[†], Hongbin Liang[*†], and Lirong Zheng[¶]

[†]MOE Laboratory of Bioinorganic and Synthetic Chemistry, State Key Laboratory of Optoelectronic Materials and Technologies, School of Chemistry and Chemical Engineering, Sun Yat-sen University, Guangzhou 510275, P.R. China.
[‡]The Hong Kong Institute of Education (The Education University of Hong Kong, designate), 10 Lo Ping Road, Tai Po, Hong Kong S.A.R., P.R. China
[§]Center for Nano Science and Technology, Department of Physics, Anhui Normal University, Wuhu, Anhui 241000, P.R. China
[¶]Beijing Synchrotron Radiation Facility, Institute of High Energy Physics, Chinese Academy of Sciences, Beijing 100039, P.R. China

Contents SI

Experimental Methods and Measurements

Materials and Synthesis. The phosphors were synthesized by a sol-gel combustion method. Firstly, the metal nitrate solutions were obtained in stoichiometric proportions by dissolving rare earth oxides in nitric acid. Anhydrous ethanol was added to the resulting solution with heating at 65 ^{o}C to evaporate superfluous water until a transparent sol was obtained. The sol was dried at 95 ^{o}C to form a dry gel which was then fired in a muffle furnace at 700 ^{o}C in air for 3 hours to obtain a precursor. After grinding, the precursor was sintered at 1400 ^{o}C for 6 h in a CO reducing atmosphere created by burning activated carbon. The product was reground, washed twice by warm dilute nitric acid and water, and finally oven-dried. The XANES (Figure S1) shows that ytterbium is present in the samples in the trivalent state even though a reducing atmosphere was employed in synthesis. In fact the PL and PLE spectra are unchanged whether an ambient air or reducing atmosphere is employed in the synthesis (Figure S2).

Instrumental Measurements. The final products were examined on a Bruker D8 Advance type powder X-ray diffractometer, using Cu Ka radiation (λ = 1.5404 Å) and operating at 40 kV and 40 mA. The UV-excitation and UV-visible emission spectra at room temperature, as well as the luminescence decay curves, were measured by a FLS920-combined Fluorescence Lifetime and Steady State Spectrometer (Edinburgh Instruments) equipped with a 450 W Xe lamp, a TM300 excitation monochromator and two TM300 emission monochromators, equipped with a red sensitive PMT for visible spectral measurements and a R5509-72 NIR-PMT in a liquid nitrogen cooled housing (Hamamatsu Photonics) for NIR spectral measurements. A 150 W nF900 flash lamp was employed for measurement of nanosecond lifetime decay curves. For lifetimes in the microsecond and millisecond range a 60W uF900 flash lamp with a pulse width of 1.5–3.0 μs and a pulse repetition rate of 50 Hz was employed.
The Yb X-ray absorption near-edge structure (XANES) analysis (Fig. S1) was carried out in the fluorescence mode at room temperature on the beamline 1W2B of the Beijing Synchrotron Radiation Facility (BSRF). The oxidation state detected in all samples is +3. The excitation and emission spectra of samples prepared in an ambient or reduced atmosphere are similar (Fig. S2).

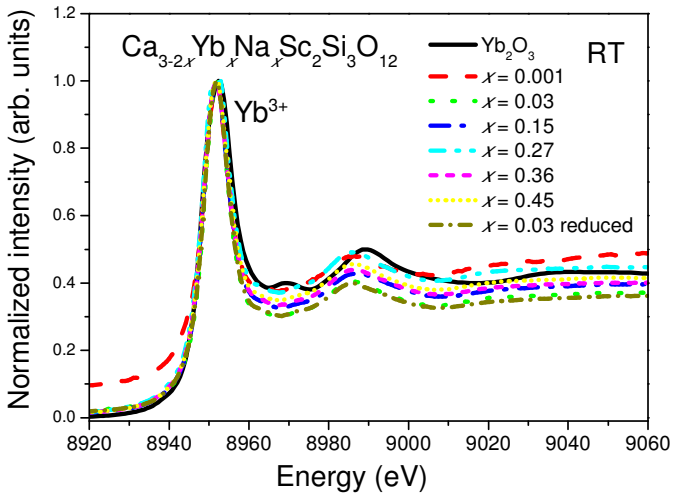

Fig. S1. Yb-L3 X-ray Absorption Near-edge Structure in $Ca_{3-2x}Yb_xNa_xSc_2Si_3O_{12}$ Samples.

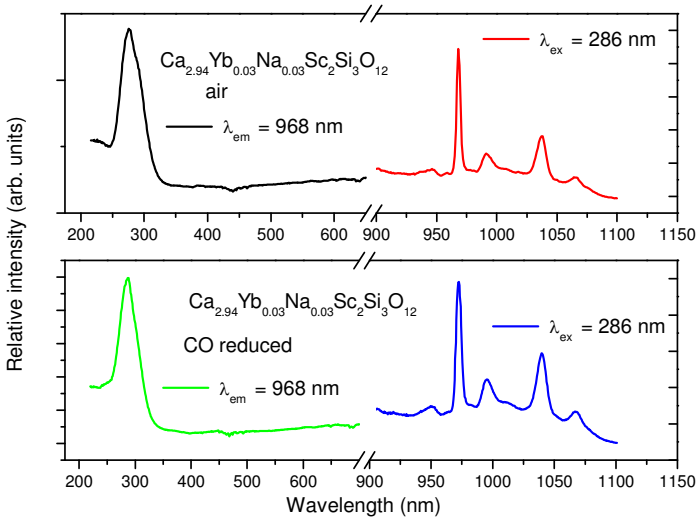

Fig. S2. The Excitation and Emission Spectra of $Ca_{2.94}Yb_{0.03}Na_{0.03}Sc_2Si_3O_{12}$ Synthesized Under Air and CO Reduced Atmosphere.

Evidence That Yb^{3+} Substitutes at the Ca^{2+} and Not the Sc^{3+} Site. The electronic spectra of several lanthanide ions diluted into the $Ca_3Sc_2Si_3O_{12}$ host have been reported and it has been demonstrated that Ln^{3+} substitutes at the Ca^{2+} site of D_2 point group symmetry.[S1,S2] The Yb^{3+} ion is slightly smaller than the Eu^{3+} or Tb^{3+} ions so that some additional proof may be required to show that it does not substitute at the Sc^{3+} site. Therefore, we synthesized $Ca_3Sc_{2-x}Yb_xSi_3O_{12}$ ($x = 0.03$) and compared the X-Ray diffractogram as in Figure S3 below. It is evident that Sc_2O_3 and SiO_2 are produced in this case, but not for $Ca_{3-2x}Sc_2Yb_xNa_xSi_3O_{12}$ ($x = 0.03$).

Figure S4 shows the Yb^{3+} emission spectra of samples prepared with starting stoichiometries for Yb^{3+} substituting at the Ca^{2+} or Sc^{3+} sites. The spectra are very similar.

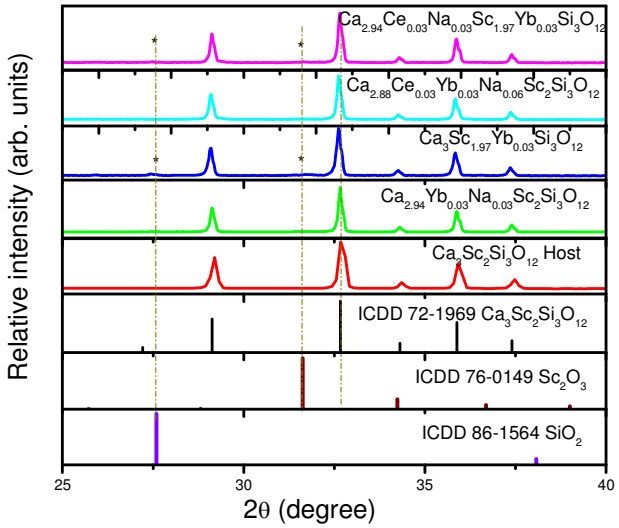

Fig. S3. X-ray Diffractograms of Ce, Yb, and Na-substituted $Ca_3Sc_2Si_3O_{12}$ Host.

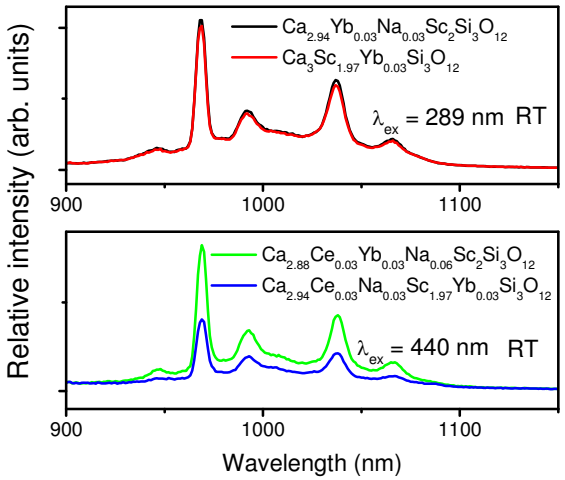

Fig. S4. Yb^{3+} Emission Spectra at RT of Yb- and Ce, Yb-doped $Ca_3Sc_2Si_3O_{12}$.

Artefact in Lifetime Measurements. For 289 nm excitation of CSS:Yb_xNa_x (and CSS:$Ce_{0.1}Yb_xNa_{x+0.1}$), in addition to excitation at 440 nm and 896 nm, we observe a biexponential decay of Yb^{3+} emission with a rise lifetime of ~9.7 μs. Since this phenomenon also occurs during direct excitation at 896 nm, it is attributed to the instrumental response using NIR detection. The decay curves of the $^2F_{5/2}$ *J*-multiplet of CSS:$Yb_{0.27}Na_{0.27}$ at 3 K are shown in Figure S5. On taking into account this artifact, the lifetime decay at RT is monoexponential but a slight decrease from 0.97±0.04 ms to 0.86±0.03 ms is observed for the (different) direct $^2F_{5/2}$ population mechanism when the excitation wavelength changes from 289 nm to 884 or 896 nm.

Ce^{3+} Lifetime at 77 K. At 77 K, with excitation at 440 nm and emission at 550 nm, the lifetime of Ce^{3+} in CSS:$Ce_{0.1}Yb_{0.03}Na_{0.13}$ can be fitted by a monoexponential function (τ = 58.1±0.2 ns R^2_{adj} = 0.9964), or a biexponential function with similar results to that in Table 1 for this sample (τ_1 = 66.9±1.3 ns, τ_2 = 26.8±2.5 ns, R^2_{adj} = 0.9970).

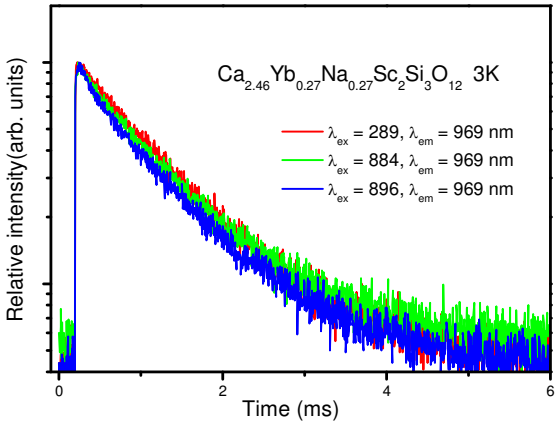

Fig. S5. The Emission Decay Curves of CSS:$Yb_{0.27}Na_{0.27}$ at 3 K.

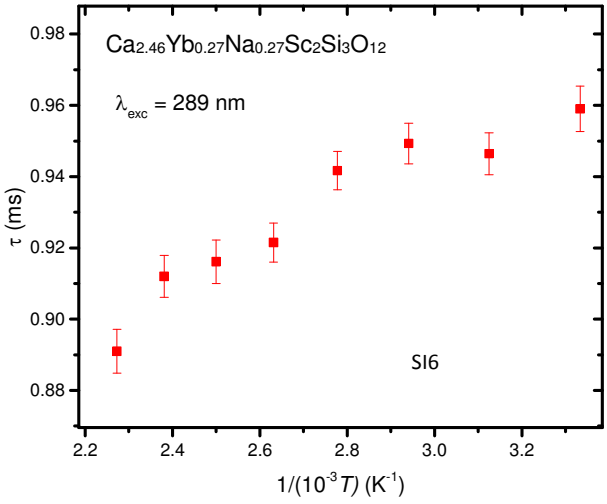

Fig. S6. Temperature Dependence of the Yb^{3+} Lifetime of CSS:$Yb_{0.27}Na_{0.27}$ Upon CT Excitation.

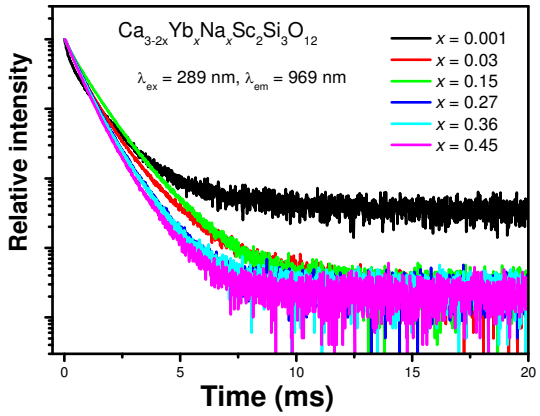

Fig. S7. Room Temperature Decay Curves of the $^2F_{5/2}$ State as a Function of Yb^{3+} Concentration in CSS:Yb_xNa_x.

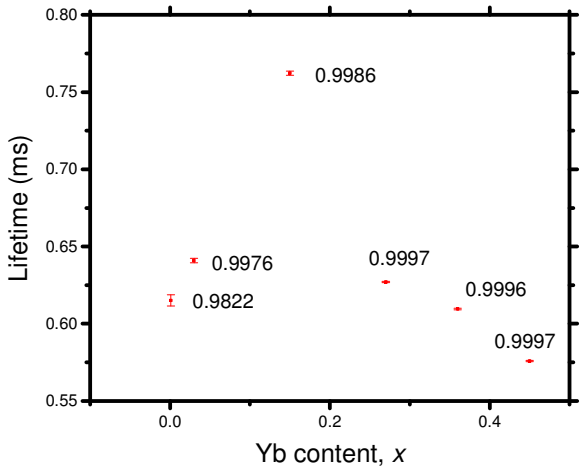

Fig. S8. Room Temperature Monoexponential Lifetimes of the Yb^{3+} $^2F_{5/2}$ *J*-multiplet as a Function of Yb Concentration in CSS:Yb_xNa_x. The Numbers are the Adjusted Coefficients of Determination, R^2_{adj}, For the Fits. (λ_{exc} = 289 nm, λ_{em} = 969 nm)

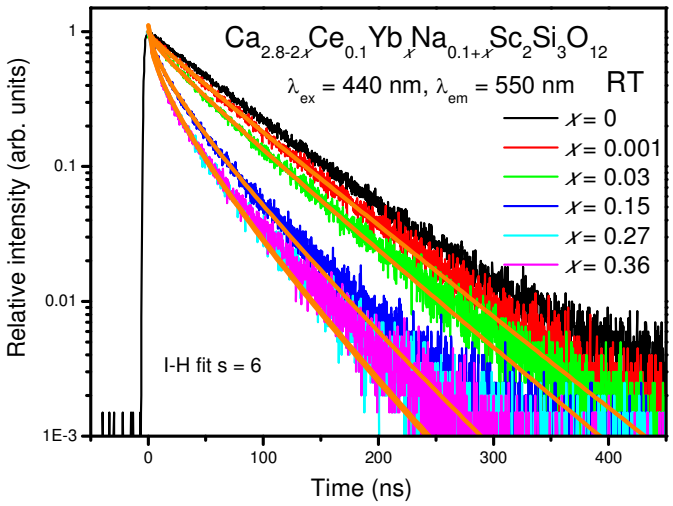

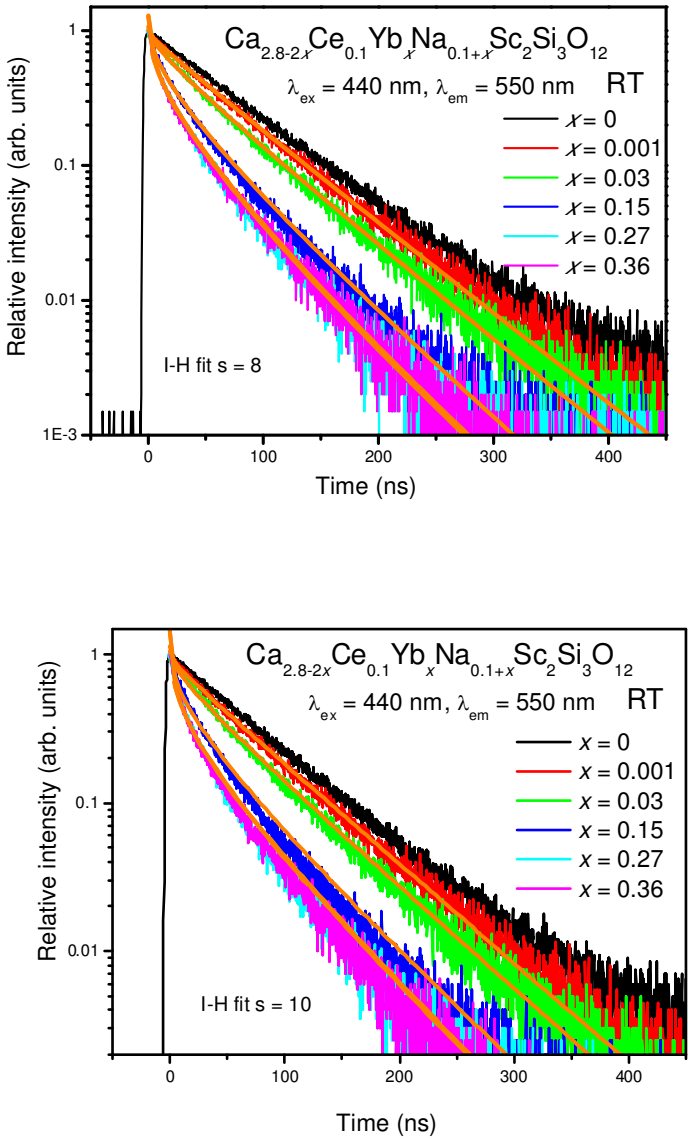

.

Fig. S9. Inokuti-Hirayama Fits to the RT Ce^{3+} Emission in CSS:$Ce_{0.1}Yb_xNa_{0.1+x}$ for s = 6, 8 and 10

$Ca_{2.8-2x}Ce_{0.1}Yb_xNa_{0.1+x}Eu_xSc_2Si_3O_{12}$		
xYb^{3+}	R_{adj}^2	C_A/C_0
0	0.9984	-
0.001	0.9984	0.14
0.03	0.9979	0.33
0.15	0.9949	0.95
0.27	0.8437	1.24
0.36	0.9932	1.25

Table S1. Inokuti-Hirayama Fitting Parameters for $s = 8$.

Analysis of Energy Transfer in CSS:$Ce_{0.1}Yb_xNa_{x+1}$ Using the Dornauf-Heber Model[S3]

The acceptor Ca^{2+} lattice points are arranged in spherical coordination shells around the $Yb^{\bullet}_{Ca}$ donor, where N, the number of acceptors per unit volume is approximated by its mean value Zx, where, as previously, x is the molar concentration and Z is the sum over k shells where shell l has ${}^lZ$ sites. The donor-acceptor distance in the lth shell is ${}^lR$. Then for multipole-multipole interactions (index s), the change of intensity with time is given by:

$$\phi_{EX}(t) = \exp\left\{-\frac{t}{\tau_0}\right\}\cdot\exp\left\{-\frac{t\cdot 4\pi c_A\cdot R_0^S}{\tau_0\left(S-3\right)^{k+1}R^{S-3}}\right\}$$
$$\times\left[\sum_{l=1}^{k}\frac{{}^lZ}{Z}\cdot\exp\left\{-\frac{t}{\tau_0}\cdot\left(\frac{R_0}{{}^lR}\right)^S\right\}\right]^{Z\cdot x}$$

where τ_0 = 66.8 ns; c_A is the acceptor (Yb^{3+}) concentration = (x×8/1837.8); R_0 is the critical transfer radius (Å); and the particulars for the shells are listed in Table S2. The fitted values of R_0 are listed in Table S3.

Shell	Coordination number	Distance (Å)
1	4*x*	3.7508
2	8*x*	5.7294
3	2*x*	6.1250
4	8*x*	6.8480
5	4*x*	7.1822
6	8*x*	8.3870
7	4*x*	8.6621
8	12*x*	9.4393
9	8*x*	10.3854
10	8*x*	10.6088
11	8*x*	11.0420
12	16*x*	11.2523
13	16*x*	12.0571
14	6*x*	12.2500
15	8*x*	12.8114
16	8*x*	13.5236
17	8*x*	13.6959
18	16*x*	14.0341
19	20*x*	14.2002
20	16*x*	14.8460
21	8*x*	15.0031
22	8*x*	15.4649
23	24*x*	16.0599
24	24*x*	16.4921
25	12*x*	16.6336
26	24*x*	17.1882
27	12*x*	17.3241
28	28*x*	17.7255
29	8*x*	18.2470
30	10*x*	18.3750
31	8*x*	18.6285
32	20*x*	18.7539
33	16*x*	19.2475
34	8*x*	19.3689
35	20*x*	19.7288

Table S2. Ce^{3+} Donor - Yb^{3+} Acceptor Shell Distances and Coordination Numbers in CSS.

In the case of exchange interaction:

$$\phi_{EX}(t) = \exp\left\{-\frac{t}{\tau_0}\right\}\cdot\exp\left\{-\frac{t\cdot 4\pi c_A}{\tau_0}\right.$$
$$\left.\times\left(\frac{^{k+1}R^2}{\gamma}+2\frac{^{k+1}R}{\gamma^2}+\frac{2}{\gamma^3}\right)\cdot\exp\left\{\gamma\left(R_0-{}^{k+1}R\right)\right\}\right\}$$
$$\times\left[\sum_{l=1}^{k}\frac{^{l}Z}{Z}\cdot\exp\left\{-\frac{t}{\tau_0}\cdot\exp\left\{\gamma\left(R_0-{}^{l}R\right)\right\}\right\}\right]^{Z\cdot x}$$

where γ has the dimension L^{-1}.

There is only one variable parameter, R_0. In the case of CSS:$Ce_{0.1}Yb_xNa_{0.1+x}$, the fittings for multipole interactions are superior for s = 8 and are displayed below for 15 shells:

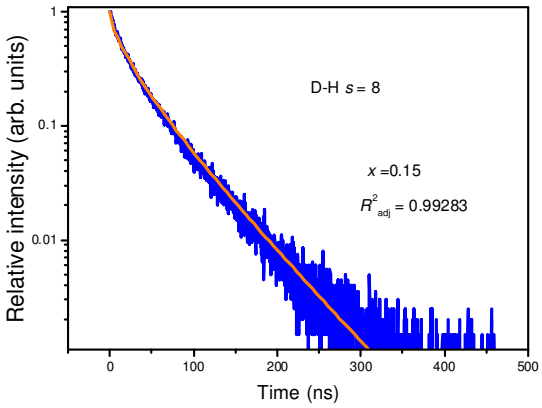

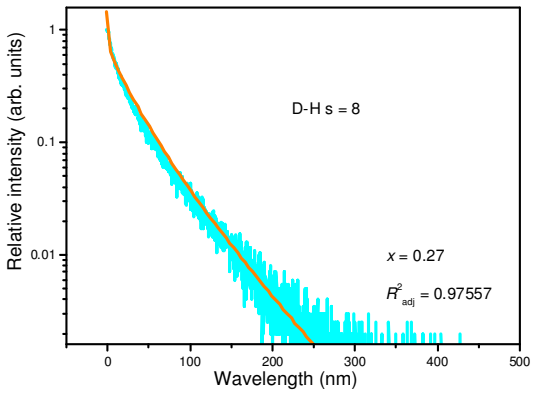

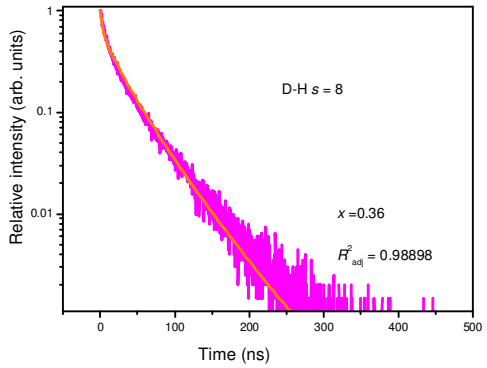

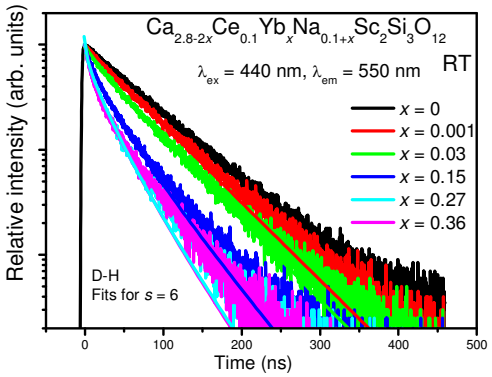

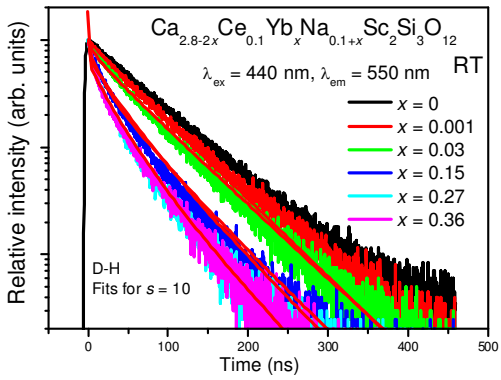

Fig. S10. Energy Transfer in CSS:$Ce_{0.1}Yb_xNa_{x+1}$ Using the Dornauf-Heber Model:[S3] Individual Fits for s = 8 For Different Yb^{3+} Concentrations and Fits For s = 6 and 10.

x	R_0 (Å)
0.03	7.55±0.01
0.15	6.38±0.01
0.27	5.88±0.01
0.36	5.56±0.01

Table S3. Dornauf-Heber Parameter R_0 for Fits With s = 8.

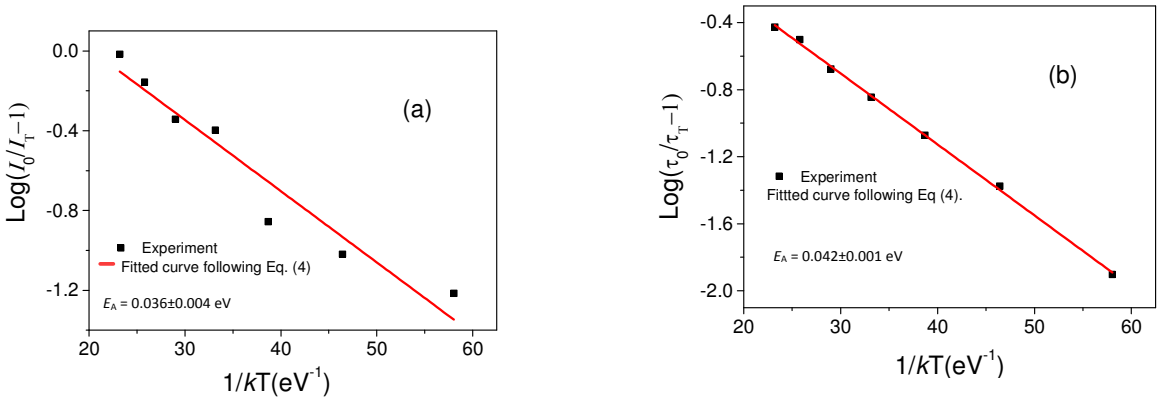

Fig. S11. The Fits Using Eq. (5) of Emission Intensities (a) and Lifetimes (b) as a Function of Temperature Dependence For Ce^{3+} in CSS:$Ce_{0.1}Yb_{0.03}Na_{0.13}$. ($\lambda_{exc}$ = 440 nm, λ_{em} = 550 nm).

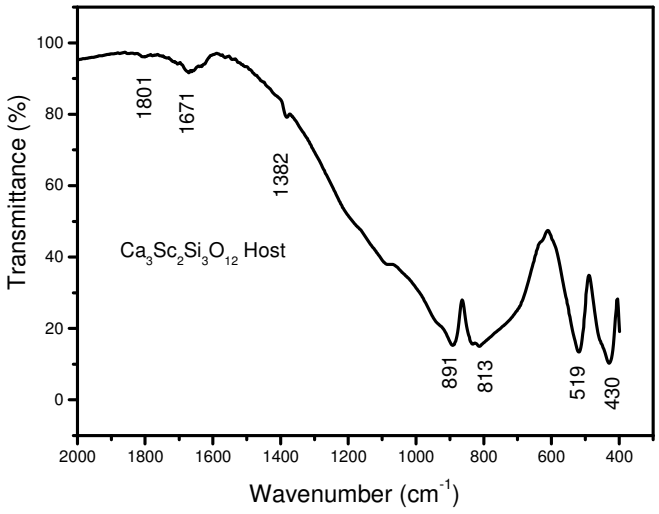

Fig. S12. FT-IR Spectrum of CSS Host at Room Temperature.

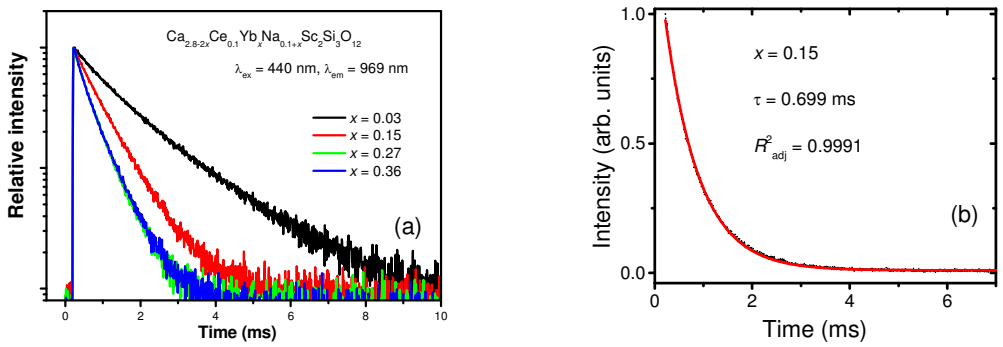

Fig. S13. (a) The Decay Curves of Yb^{3+} Emission at 969 nm Under Excitation of Ce^{3+} at 440 nm For Different Yb^{3+} Concentration Samples at RT; (b) Monoexponential Fit For the Decay of $x = 0.15$.

Decay of Yb^{3+} Emission in CSS:$Ce_{0.1}Yb_xNa_{0.1+x}$. Figure S13(a) presents the decay curves of Yb^{3+} $^2F_{5/2} \rightarrow {}^2F_{7/2}$ emission of CSS: $Ce_{0.1}Yb_xNa_{0.1+x}$ under excitation of 440 nm at RT. The fitting with a monoexponential function for $x = 0.15$ is shown in Figure S13(b). The fit of $x = 0.03$ gives the decay time of 1.36 ms and this decreases to 0.455 ms when $x = 0.36$. Under 440 nm excitation at 77 K, the lifetime of Yb^{3+} for $x = 0.03$ (i.e., $Ca_{2.74}Ce_{0.1}Yb_{0.03}Na_{0.13}Sc_2Si_3O_{12}$) emission measured at 969 nm is similar 1.267±0.004 ms ($R^2_{adj} = 0.9967$) (Figure S14). This figure shows that direct excitation at 896 nm gives a fast component superimposed upon this lifetime, which could be due to Yb^{3+} defect site emission. However, the important result observed from this figure is that excitation at 289 nm into the CT band gives Yb^{3+} emission at the same wavelength of 969 nm with a lifetime of 0.630±0.005 ms ($R^2_{adj} = 0.9711$). This is one-half of the lifetime under 440 nm excitation. It is also shorter than the RT lifetime of CSS:$Yb_{0.03}Na_{0.03}$ where Ce^{3+} is absent: 1.005±0.003 ms ($R^2_{adj} = 0.9982$). It is therefore clear from the different lifetimes of the decay curves of $Ca_{2.74}Ce_{0.1}Yb_{0.03}Na_{0.13}Sc_2Si_3O_{12}$ at 77 K under 289 nm and 440 nm excitation that different excitation mechanisms are operative in these cases. In fact, the former excitation wavelength has been associated with Ce^{3+} ions at minority sites[S4] so that a different energy transfer scenario is operative in this case and it requires further investigation.

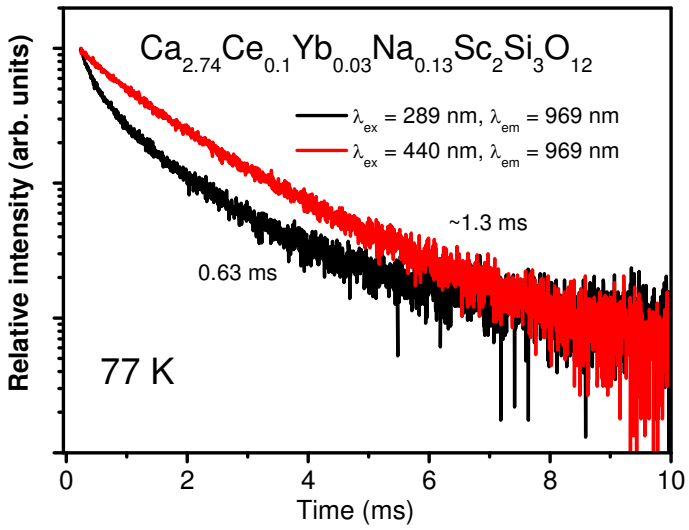

Fig. S14. The Decay Curves of Yb^{3+} Emission in CSS:$Ce_{0.1}Yb_{0.03}Na_{0.13}$ at 77 K.

Contributions of Dipole-dipole and Dipole-quadrupole Energy Transfer Mechanisms to the Total Energy Transfer Rate

Kushida[S5] generalized the theory of energy transfer (ET) to calculate the average rate $\overline{P}_{AB}$ of ET between the manifolds J_a and J_b by summing over all the possible terminal crystal field (CF) states $|a'b'>$ and taking the Boltzmann-weighted average of the initially occupied CF states, $|ab>$:

$$\overline{P}_{AB} = \frac{2\pi}{\hbar}\overline{J^2}\,\overline{S}, \qquad (1)$$

and:

$$\overline{J^2} = \frac{1}{[J_a][J_b]}\sum_{\substack{a,b\\a',b'}} |< ab \,|\, H_{AB} \,|\, a'b' >|^2 \qquad (2)$$

is the 'squared electronic transition element', averaged over the initial crystal field (CF) states but summed over the terminal CF states, for ET between the J_a'

$J_b^{'}$ manifolds and

$$\overline{S} = \frac{1}{[J_a^{'}][J_b^{'}]} \sum_{\substack{a,b \\ a',b'}} Y_a Y_b \int g_{aa'}(E) g_{bb'}(E) \mathrm{d}E \qquad (3)$$

is the averaged overlap integral between individual CF emission and individual CF absorption transitions, in which $[J] = 2J + 1$, Y is a normalized Boltzmann factor, and g is a line shape function. Here, $a = Ce^{3+}$, $b = Yb^{3+}$. The typical value of $\overline{S}$ at room temperature is 1×10^{-3}/cm^{-1}.[S5] In the present case, for multiphonon $\overline{S}$ assisted ET, is given by an expression from Wassam and Fong[S6] and it is not necessary to include it here since we are taking a ratio.

Since the Ce^{3+} $5d^1 \rightarrow 4f^1$ transition is electric dipole allowed, the possible multipolar mechanisms for $Ce^{3+} \rightarrow Yb^{3+}$ ET are dipole – quadrupole (dq) or dipole – (forced) electric dipole (dd). The $\overline{J^2}$ can be calculated for these two mechanisms by the formulae as follows:

$$\overline{J^2} = \frac{1}{[J_a][J_b]} \left(\frac{2}{3}\right) \left(\frac{e^4}{R^6}\right) \left[< J_a \mid D^{(1)} \mid J_a^{'} >^2 \right] \left[\sum_{\lambda} \Omega_{B\lambda} < J_b \| U^{(\lambda)} \| J_b^{'} >^2 \right]$$

$$\overline{J^2} = K \left(\frac{2}{3}\right) \left(\frac{1}{R^6}\right) \left[\sum_{\lambda} \Omega_{B\lambda} < J_b \| U^{(\lambda)} \| J_b^{'} >^2 \right]$$

or

$$\overline{J^2} = K \left(\frac{2}{3}\right) \left(\frac{1}{R^6}\right) 2 \times 10^{-20} \qquad (4)$$

for (dd) interaction between the donor and acceptor with separation R; is the reduced $< J_b \| U^{(\lambda)} \| J_b^{'} >$ matrix element of the unit tensor $U^{(\lambda)}$; and Ω_λ (λ = 2, 4, 6) is the Judd parameter obtained by fitting manifold–manifold ED transition intensities. The reduced matrix elements are

$<^2F_{5/2}\| U^{(2)}\|^2F_{7/2}>^2$ = 6/49, $<^2F_{5/2}\| U^{(4)}\|^2F_{7/2}>^2$ = 20/49 and

$<^2F_{5/2}\| U^{(6)}\|^2F_{7/2}>^2$ = 6/7.[S5]

The values for Ω_λ parameters for Yb^{3+} are scarce. Ω_2 was given between 0.93-36.9×10^{-20} cm^2, Ω_4 as 1.6×10^{-20} cm^2; Ω_6 as 1.6×10^{-20} cm^2.[S7] This gives a value of $\sum_\lambda \Omega_\lambda <^2F_{7/2}\| U^\lambda \|^2F_{5/2}>^2$ between (2.1-6.5)×10^{-20} cm^2.

Kushida gives the value for Yb^{3+} = 2×10^{-20} cm^2 which we adopt here.[S5]

The corresponding formula for dq interaction is:

$$\overline{J^2} = \frac{1}{[J_a][J_b]}\left(\frac{e^4}{R^8}\right)\left[< J_a \| D^{(1)} \| J_a^{'} >^2\right] < 4f \| r^2_{Yb^{3+}} \| 4f >^2 < f \| C^{(2)} \| f >^2 < J_b \| U^{(2)} \| J_b^{'} >^2$$

$$\overline{J^2} = K\left(\frac{1}{R^8}\right) < 4f \| r^2_{Yb^{3+}} \| 4f >^2 < f \| C^{(2)} \| f >^2 < J_b \| U^{(2)} \| J_b^{'} >^2$$
$$= K\left(\frac{1}{R^8}\right) 3.739\times10^{-34}\times1.867\times0.1224$$
$$= K\left(\frac{1}{R^8}\right) 8.547\times10^{-35}$$

(5)

where $< 4f \| r^2_{Yb^{3+}} \| 4f >$ = 0.691 a.u. = (0.691× 5.29×10^{-9})^2 = 1.9337×10^{-17} cm^2;

$$< f \| C^{(2)} \| f > = (-7) \begin{pmatrix} 3 & 2 & 3 \\ 0 & 0 & 0 \end{pmatrix} = (-7)\ 0.195180014 = -1.366260098.$$

The total ET rate is:

$$\overline{P}_{total} = \sum_{shells} \overline{P}_{AB}(R) N C_{Yb} P \quad \textbf{(6)}$$

where $\overline{P}_{AB}(R)$ is the ET rate for Ce^{3+} - Yb^{3+} transfer at the separation R, N is the number of acceptor ions in the shell, C_{Yb} is the concentration of Yb doping, and P is the probability that the acceptor ion is in the initial state at the relevant ET process.

From the crystal structure, R_1 = 3.7508 Å = 3.7508×10^{-8} cm, N_1 = 4, etc., so

$$\overline{P}_{total} = \sum_{shells} \overline{P}_{AB}(R) N C_{Yb} P = [4\left(\frac{1}{3.7508\times10^{-8}}\right)^6 + 8\left(\frac{1}{5.7294\times10^{-8}}\right)^6 + ..]C_{Yb}P = 0.00191\times10^{48}\overline{P}_{AB}C_{Yb}P \quad (7)$$

(cm^{-6} units for 1/R^6)

For dd transfer, up to 35 shells.

$$\overline{P}_{total} = \sum_{shells} \overline{P}_{AB}(R) N C_{Yb} P = [4\left(\frac{1}{3.7508\times10^{-8}}\right)^8 + 8\left(\frac{1}{5.7294\times10^{-8}}\right)^8 + ..]C_{Yb}P = 0.000113212\times10^{64}\overline{P}_{AB}C_{Yb}P \quad (8)$$

(cm^{-8} units for 1/R^8) for dq transfer up to 35 shells.

So for up to 35 shells: $$\frac{\overline{P}_{total(dd)}}{\overline{P}_{total(dq)}} = \frac{1.91\times10^{45}}{1.13212\times10^{60}} \times \frac{1.333\times10^{-20}}{8.547\times10^{-35}} = 0.263$$

References

(S1) Piccinelli, F.; Speghini, A.; Mariotto, G.; Bovo, L.; Bettinelli, M. Visible Luminescence of Lanthanide Ions in $Ca_3Sc_2Si_3O_{12}$ and $Ca_3Y_2Si_3O_{12}$. *J. Rare Earths* **2009**, *27*, 555-559.

(S2) Bettinelli, M.; Speghini, A.; Piccinelli, F.; Neto, A. N. C.; Malta, O. L. Luminescence Spectroscopy of Eu^{3+} in $Ca_3Sc_2Si_3O_{12}$. *J. Lumin.* **2011**, *131*, 1026-1028.

(S3) H. Dornauf and J. J. Heber, Concentration-dependent Fluorescence-quenching in $La_{1-x}Pr_xP_5O_{14}$. *J. Lumin*. **1980**, *22*, 1-16.

(S4) Zhou, L.: Zhou, W.; Pan, F.; Shi, R.; Huang, L.; Liang, H.; Tanner, P. A.; Du, X.; Huang, Y.; Tao, Y.; Zheng, Spectral Properties and Energy Transfer of a Potential

Solar Energy Converter. *Chem. Mater*. **2016**, *28*, 2834-2843.

[S5] Kushida, T. Energy Transfer and Cooperative Optical Transitions in Rare-earth Doped Inorganic Materials. I. Transition Probability Calculation. *J. Phys. Soc. Japan* **1973**, *34***,** 1318-1337.

[S6] Wassam, W. A.; Fong, F. K. Nonresonant Energy Transfer Interactions Between Randomly Distributed Guest Molecules in Host Lattices. *J. Chem. Phys*. **1976**, *65*, 3102-3107.

[S7] Görller-Walrand, C.; Binnemans, K. Spectral Intensities of f-f Transitions. In: Handbook on the Physics and Chemistry of Rare Earths, Vol. 25 Chapter 167, 1998, Eds. Gschneidner, K. A.; Eyring, L. Elsevier Science BV, pp. 100-264.